Slater-Pauling-like Behavior of Spin Hall Conductivity in Pt-based Superlattices

Abdul-Muizz Pradipto[1,2] & Kohji Nakamura[2]

[1]Physics Study Program, Faculty of Mathematics and Natural Sciences,
Institut Teknologi Bandung, Bandung, 40132, Indonesia
[2]Department of Physics Engineering, Mie University, Tsu, Mie 514-8507, Japan
E-mail: a.m.t.pradipto@gmail.com

Abstract. The intrinsic spin Hall effect in the bulk systems of late $5d$ transition metals (Os, Ir, Pt, and Au) as well as the Pt-based superlattices were investigated by using first-principle calculations. By comparing the computed spin Hall conductivities of Pt−M superlattices (M=Os, Ir, and Au) with different compositions and those obtained from atomic bulk composition, we saw that the spin Hall conductivities (SHCs) follow the behavior described by the Slater-Pauling curve, the maximum of which is at pure Pt bulk. From the examination of the band structures of the considered systems, we found that the origin of this behavior comes from the variation of the band structures as a direct consequence of the change of the number of electrons and hybridization effects.

Keywords: *density functional theory; Pt-based superlattices; Slater-Pauling curve; Spin Hall Effect; spintronics.*

1 Introduction

The spin Hall effect (SHE) [1-3] has been largely explored in the past decade due in part to the extensive development of spintronics technology. Among the most important factors that govern the large interest in SHE is that, together with the inverse spin Hall effect (ISHE) [4], it provides an efficient route for the detection and generation of spin current [5]. It is generally accepted that SHE shares the same mechanism as the anomalous Hall effect (AHE) [6,7] in that it may consist of an intrinsic mechanism originating solely from the interactions between different electronic states of the material and extrinsic mechanisms related to the existence of impurity states [8-10]. A great number of efforts can be found in the literature to discover materials with powerful intrinsic SHEs as well as to understand the basic underlying mechanisms. Promising candidates for such materials are those containing $5d$ heavy metal elements [11-13], as they are expected to possess strong spin-orbit coupling (SOC). Among these materials, attention has been given to Pt-based systems, in which a remarkably large SHE in pure platinum has been demonstrated both experimentally and theoretically [14-18].

Received May 25th, 2021, Revised September 23rd, 2021, Accepted for publication September 24th, 2021

DOI: 10.5614/j.math.fund.sci.2021.53.3.3

Additionally, theoretical approaches to investigate SHE due to nonmagnetic impurities, i.e. SHE by extrinsic origins, show clear dependencies on the number of d electrons, n_d [11,19], although different results have been obtained in these works, which may be ascribed to the different treatment of local correlations for the d orbitals of the impurities [12]. However, detailed inspection of the nature of SHE indicates the domination of intrinsic contribution to SHE in metals [20,21] as well as in alloys, such as Au_xPt_{1-x} [22]. For this contribution, measurements on SHE in several $4d$ and $5d$ elements demonstrated a clear sign change of spin Hall conductivities (SHCs) depending on the number of d electrons [21], in which the sign change is attributed to the electron fillings of the d orbitals. The results agree with previous theoretical tight binding calculations [20] and suggest a direct relation between intrinsic SHE and n_d.

In ferromagnetic metals, several fundamental properties, such as magnetization and Curie temperature, have been understood to follow the so-called Slater-Pauling curve [23-25]. This Slater-Pauling behavior provides simple intuitions to understand the magnetic properties, as it summarizes how they depend on the number of electrons in a material. While similar behavior for the transport properties has been anticipated in $3d$ alloy systems [26], we are not aware of such reports for SHE. In this work, we re-examined the intrinsic spin Hall effect of the pure late $5d$ elements (TM=Os, Ir, Pt, and Au), where the valence electrons vary between 8 and 11, as well as the SHE of multilayer systems composed by these elements. We employed first-principle calculations and focused on spin Hall conductivity (SHC) as a quantity to describe the SHE by utilizing the Kubo formula, which is routinely used in first-principle calculations on intrinsic Hall conductivities [15]. Our results suggest that for SHC there is a close resemblance to Slater-Pauling behavior with the maximum spin Hall conductivity at pure Pt with $n_d = 9$. We expect this work to further advance our understanding of the nature of intrinsic SHE.

2 Calculation Methods

Calculations have been carried out by using the full-potential linearized augmented plane wave (FLAPW) method [27] combined with a generalized gradient approximation (GGA) [28] to the density functional theory. We considered a face-centered cubic structure for the bulk Os, Ir, Pt, and Au, as well as for the Pt(111)-based superlattices in order to investigate the dependence of the obtained spin Hall conductivities on the number of valence electrons of the systems. To model these superlattices, we considered two- and four-layered Pt-M (M=Os, Ir, and Au) models. The latter models were chosen with the following atomic alignments: (i) Pt/M/M/M (denoted hereafter as

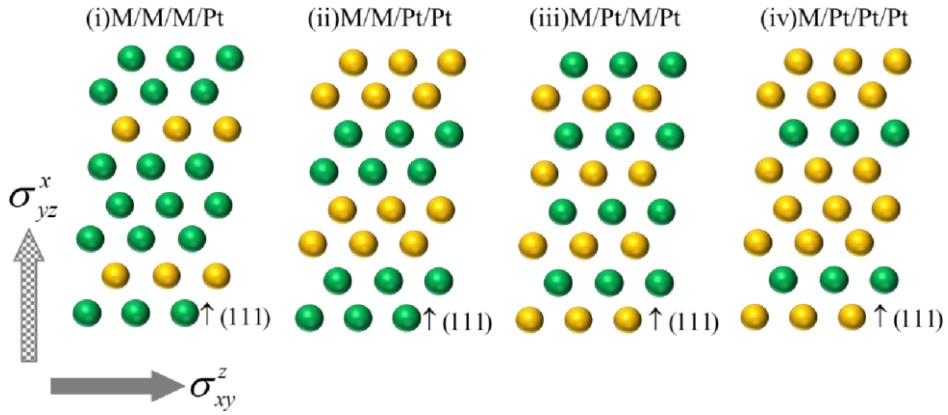

Figure 1 The four types of four-layered Pt-M superlattices assumed in the calculations: (i) Pt/M/M/M (or PtM3), (ii) Pt/Pt/M/M, (iii) Pt/M/Pt/M, and (iv) Pt/Pt/Pt/M (or Pt3M).

PtM_3), (ii) Pt/Pt/M/M, (iii) Pt/M/Pt/M, and (iv) Pt/Pt/Pt/M (or Pt_3M) (see Figure 1). These choices of the superlattices allow us to systematically modify the number of valence electrons in the systems. For instance, in four-layered Pt-Os superlattices, one can have a total of 34 (in $PtOs_3$) to 38 (in Pt_3Os) valence electrons in the unit cells containing four atomic layers.

The lattice constants of the bulk and superlattice systems were assumed to be 3.97 Å to match the optimized bulk Pt value. Test calculations performed at different crystal structures only showed insignificant modifications to the computed SHC; therefore, we chose to use the same lattice constants for all systems to focus more on the electronic contributions. A FLAPW basis with a cut-off of $|\mathbf{k}+\mathbf{G}| \leq 3.9$ a.u.$^{-1}$ and muffin-tin (MT) sphere radii of 2.4, 2.4, 2.4, and 2.3 a.u. for Os, Ir, Pt, and Au atoms, respectively, were used.

In three-dimensional materials, as in bulk structures, different SHCs along different directions can be specified and defined using the SHC tensor:

$$\sigma^s = \begin{pmatrix} 0 & \sigma^s_{xy} & \sigma^s_{xz} \\ \sigma^s_{yx} & 0 & \sigma^s_{yz} \\ \sigma^s_{zx} & \sigma^s_{zy} & 0 \end{pmatrix} \quad (1)$$

where σ^s_{ji} denotes the SHC that induces the spin current along the i-direction due to the charge current moving along the j-direction, with the spin magnetized in the k-direction. However, due to the symmetry within the xy-plane of the film, only two non-identical SHCs can be distinguished, σ^s_{xy} and σ^s_{yz}, where the z-axis is the direction perpendicular to the plane (as shown in Figure 1). These SHCs were obtained based on linear response theory by using

the calculated eigenvectors and utilizing the Kubo-formula, which is the sum of the Berry-curvature [15]:

$$\sigma_{ji}^{s} = \frac{e}{\hbar}\sum_{\mathbf{k}}\sum_{n,n'\neq n} f_{\mathbf{k}n}\frac{2\mathrm{im}\left[\langle \mathbf{k}n|\hat{j}_i|\mathbf{k}n'\rangle\langle \mathbf{k}n'|\hat{v}_j|\mathbf{k}n\rangle\right]}{(\varepsilon_{\mathbf{k}n}-\varepsilon_{\mathbf{k}n'})} \quad (2)$$

where e is the electron charge, $\hbar$ is the Planck constant, and $f_{\mathbf{k}n}$ is the Fermi distribution function for the sum of all filled bands. The $\hat{j}_i$ is the spin current operator, $\hat{v}_j$ is the velocity operator, and $\varepsilon_{\mathbf{k}n}$ and $\varepsilon_{\mathbf{k}n'}$ are calculated eigenvalues. For simplicity, the superscript 's' will be dropped from σ_{ji} in the discussions that follow.

3 Results and Discussion

3.1 Dependence of SHC on the Number of d Electrons

Table 1 Calculated spin Hall conductivities σ_{xy} and σ_{yz} in $(\Omega\cdot\mathrm{cm})^{-1}$ for the considered bulk $5d$ systems: Os, Ir, Pt, and Au.

Bulk system	$\sigma_{xy} = \sigma_{yz}$
Os	-945.79
Ir	268.02
Pt	2372.36
Au	590.88

We start by presenting the results for pure bulk systems. The calculated in-plane and out-of-plane spin Hall conductivities, σ_{zy} and σ_{yz}, are summarized in Table 1. These obtained values are in good agreement with results presented previously [15], confirming the intrinsic character of SHC in these systems. Additionally, in Os we obtained a negative SHC compared to that in Pt, which is commonly considered to possess a large SHC. The SHC gradually increases and the sign of the SHC changes, going from a negative value in Os to a small positive SHC in Ir, then reaches a peak in Pt, before further decreasing in Au. The sign change of SHCs for different atoms having different n_d resembles those predicted both theoretically and experimentally [20,21].

To further explore the dependence of SHC on the number of d electrons, we doubled the Pt cells along the c direction and replaced the second Pt with other $5d$ metals to generate two-layer Pt-based multilayers. A particularly interesting case is that of PtOs, in which 18 valence electrons are contained, similar to that of a double cell of Ir. At this point, it is important to note that for PtOs, the two components SHCs, i.e. the σ_{xy} and σ_{yz}, are different by about 519 $(\Omega\cdot\mathrm{cm})^{-1}$ and

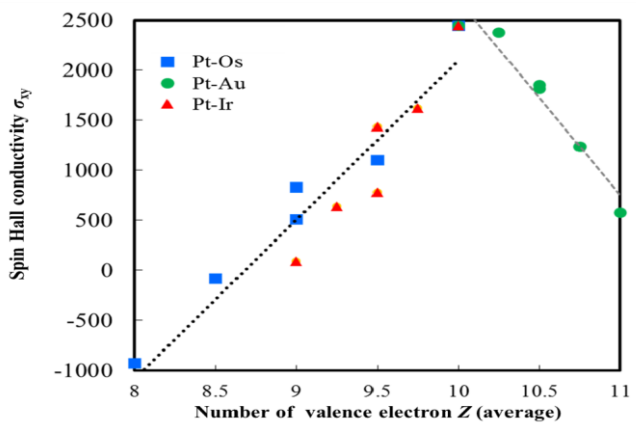

Figure 2 Plot of obtained SHC parameter \sigma_{xy} in (Ω·cm)−1 as a function of the average number of valence electrons.

211 $(\Omega \cdot \mathrm{cm})^{-1}$, respectively, although both are comparable to the values obtained for Ir, which are much smaller than those of Pt.

3.2 Slater-Pauling behavior of SHC

The regularity of the computed SHC with the number of $5d$ electrons suggests that there is a relation resembling the Slater-Pauling behavior, which is well-established for describing the behaviors of the Curie temperature and magnetic moment [23-25]. In order to confirm this, we further quadrupled the cells along the c direction in order to have four atoms in the unit cell and build several Pt-based 4-layered superlattices, as depicted in Figure 1. The obtained SHCs are shown in Figure 2, which summarizes the main results of this work. Firstly, the obtained SHCs of the end structures of all superlattice multilayers, i.e. Pt_4 and M_4, again reproduced well the values obtained from the single cell calculations.

Insignificant deviations nevertheless occurred, for instance in the Pt system, in which the calculated SHC for the quadruple layer was around 2500 $(\Omega \cdot \mathrm{cm})^{-1}$ compared to about 2400 $(\Omega \cdot \mathrm{cm})^{-1}$ in the single cell system. Secondly, from the zero concentration of Pt, the calculated SHCs increased almost linearly upon the increasing concentration of Pt. Again, particularly interesting systems are those of PtOs multilayers, in which the sign change of SHC can be clearly observed going from a rather large negative value in Os_4 to a very small negative SHC in $PtOs_3$, and then gradually increasing from Pt_2Os_2 towards a large positive value in the Pt_4 system. Similar systematic changes can also be observed for the PtIr- and PtAu-based systems, although obviously no sign change of SHC is involved.

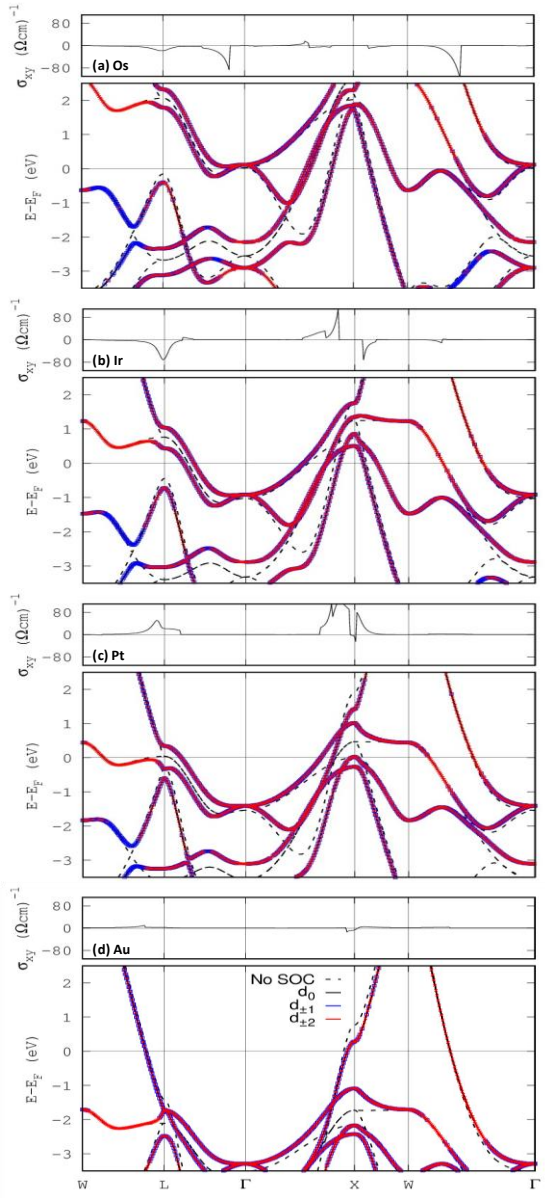

Figure 3 The k-dependent spin Hall conductivities σ_{xy} and the band structures of (a) Os, (b) Ir, (c) Pt, and (d) Au at the primitive fcc unit that contains one atom per cell. The dotted lines show the band structure without SOC, while the different colors indicate different d orbital characters to the band structure with SOC.

We should also note here that in the case of Pt_2M_2 multilayers that can be either Pt/Pt/M/M or Pt/M/Pt/M arrangements, the calculated SHCs show some

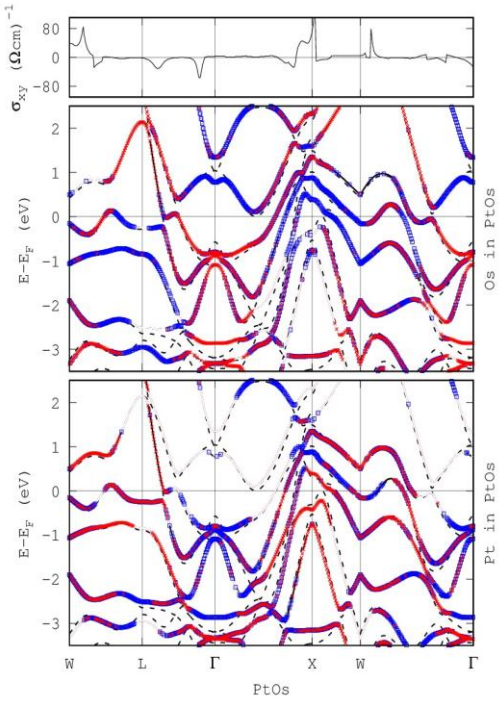

Figure 4 The k-dependent spin Hall conductivities σ_{xy} and band structures of PtOs. Blue (red) lines show the $d_{\pm 1}$ ($d_{\pm 2}$) orbital characters to the band structure with SOC.

differences in these two cases, indicating that additional effects due to atomic alignment can play a role. Although all systems possess reflection symmetry normal to the (111) direction, the reflection planes are situated differently in these Pt_2M_2 multilayers. For Pt/Pt/M/M, the reflection planes are lying in between the two Pt layers and between two M layers. On the other hand, the reflection planes in Pt/M/Pt/M are defined in each atomic layer. While the presence of reflection symmetry does not prohibit SHE, it does govern the allowed interlayer distances and overall geometry, which should moderately affect the SHE.

In Figure 3 the k-dependence of SHC is plotted together with the band structures of each system. It is obvious that the SOC induces the removal of several band degeneracies. These band splittings can be clearly observed to occur from higher energy to lower energy, going from Os to Au, due to the Fermi level shifting as a direct consequence of different numbers of electrons occupying the $5d$ bands. Such splitting takes place for instance at point K as a result of the removal of the $d_{m\pm 2}$ degeneracies, and at the point C, which mainly have a $d_{m\pm 1}$ character.

Looking at the details of each band structure, one can see from the band structure of Os displayed in Figure 3a that in the high-symmetry k-path, negative SHC comes together with the band splittings near the Fermi level in between points W and Γ or around path L−Γ, that mainly have a $d_{m\pm1}$ character, which may give rise to a totally negative SHC within the full Brillouin zone. In Figure 3b, one can also see that there are competing positive and negative contributions to the SHC located around different k-points, so that in total one could expect a small SHC value for Ir. For Pt (see Figure 3c), large contributions to the SHC, as displayed in the high-symmetry k-path, originate from the interaction of $d_{m\pm2}$ orbitals around the L and X points, as well as around the Γ−X path. Indeed, previously, the most dominant contribution to SHC in Pt has been attributed mainly to the $d_{m\pm2}$ orbitals [20]. Finally, in the case of Au, as shown in Figure 3d, there are only few electronic states around the Fermi level due to the formally fully occupied $5d$ bands within the $5d^{10}6s^{1}$ configuration. This indicates the much smaller SHC within the full Brillouin zone compared to that of Pt.

In Figure 4 the k-dependent SHC and the band structure of PtOs are plotted, showing the contributions of both Pt and Os atoms to the band structure of the multilayer. For comparison, we also plotted the band structures of the double cells of Os, Ir, and Pt having valence electrons of 16, 18, and 20, respectively. We note here that the k-dependent SHCs of the double layers Os, Ir, and Pt are obviously different from those of the respective single cells due to the cell doubling (not shown in Figure 4), however, the computed SHCs within the full Brillouin zone reproduce those of the unit cells well, indicating the robustness of our computed SHCs with respect to the k-point mesh. Indeed, when we compare the band structure of PtOs and the double cells of pure Os, Ir, and Pt, around the Γ point, the band structure of PtOs resembles to some extent that of double cell Ir. As in the case of Ir, the interactions of different bands at different k-positions lead to positive and negative SHC. Although there are strong hybridization effects taking place, it is still quite visible that the negative contributions to the SHC, such as around the Γ point, are likely due to the Os bands, while the positive contributions, for instance around the X point, have a strong Pt character. In particular, the splitting of the $d_{m\pm1}$ bands of PtOs that leads to a gap opening at the Γ point is situated at around 1 eV, which is in between that of Pt (at the Fermi level) and Os (at an energy of about 2 eV), and interestingly, this band mainly has an Os character. Also, the splitting of the band around the W−Γ path slightly above the Fermi level is dominated by Os. On the other hand, around points X and W, the highest occupied bands below the Fermi level have a Pt character, which may be ascribable to the fact that the same bands in pure Os are not occupied and situated further from the Fermi level.

This Slater-Pauling-like behavior can be explained by the variation of the electronic structures as a direct consequence of the change of the number of electrons and the hybridization effects, since the SOC strengths are expected to be of the same order of magnitude due to all elements belonging to the same $5d$ period. As shown in the PtOs systems described in Figure 4, both transition metals composing the multilayers can play equal roles in giving rise to the SHC of the multilayers. Exceptions should be mentioned, however, for the PtAu systems, in which all the $5d$ bands of Au are almost fully occupied, causing these bands to occupy well below the Fermi level. Indeed, we notice from our calculated band structures (not shown) that although some Pt bands are slightly pushed away from the Fermi level due to hybridization with the Au bands, the bands around the Fermi level mainly have a Pt character. The k-dependent SHC also shows peaks around the k points where Pt band crossings occur and, interestingly, these are also the positions of the peaks in the SHC of the pure Pt system. One can therefore conclude that the intrinsic spin Hall effects are dominated by the Pt bands, especially for PtAu multilayers.

4 Conclusion

In summary, with our first-principle calculations demonstrated qualitatively the Slater-Pauling-like behavior of the spin Hall conductivities of $5d$ transition metal bulk systems. We have shown that this behavior is closely related to the number of $5d$ electrons and, in the case of multilayer superlattices, to the modification of the band structures due to hybridization between the constituting elements. The details of the atomic arrangement are also predicted to influence the SHC, however its contribution is rather small.

Acknowledgements

We thank Takahiro Ito for our fruitful discussions with him. This work was supported by JSPS KAKENHI, Grant Numbers 15H05702, 19K03716, and 21K03444, the Cooperative Research Program of Network Joint Research Center for Materials and Devices, and Institut Teknologi Bandung through PPMI ITB 2021 research grant. The computations were mainly performed at the Research Institute for Information Technology, Kyushu University.

Nomenclature

n_d	=	number of electrons in d orbital
σ_{ji}	=	spin Hall conductivity component within the ji-plane with the spins aligned with the k-direction plane
$f_{\mathbf{k}n}$	=	Fermi distribution function

$\hat{j}_i$ = spin current operator
$\hat{v}_j$ = velocity operator
$\varepsilon_{\mathbf{k}n}$ = calculated occupied eigenvalues
$\varepsilon_{\mathbf{k}n'}$ = calculated unoccupied eigenvalues

References

[1] Dyakonov, M.I. & Perel, V.I., *Current-induced spin orientation of electrons in semiconductors*, Phys. Lett., **35A**, pp. 459-460, 1971.
[2] Hirsch, J.E., *Spin Hall effect*, Phys. Rev. Lett., **83**, p. 1834, 1999.
[3] Zhang, S., *Spin Hall effect in the presence of spin diffusion*, Phys. Rev. Lett., **83**, p. 393, 2000.
[4] Saitoh, E., Ueda, M., Miyajima, H. & Tatara. G., *Conversion of spin current into charge current at room temperature: Inverse spin-Hall effect*, Appl. Phys. Lett., **88**, p. 182509, 2006.
[5] Valenzuela, S.O. & Tinkham, M., *Direct electronic measurement of the spin Hall effect*, Nature, **442**, p. 176, 2006.
[6] Karplus, R. & Luttinger, J.M., *Hall effect in ferromagnetics*, Phys. Rev., **95**, p. 1154, 1954.
[7] Smit, J., *The spontaneous Hall effect in ferromagnetics*, I. Physica, **21**, pp. 877-887, 1955.
[8] Sinova, J., Culcer, D., Niu, Q., Sinitsyn, N.A., Jungwirth, T. & MacDonald, A.H., *Universal intrinsic spin Hall effect*, Phys. Rev. Lett., **92**, p. 126603, 2004.
[9] Nagaosa, N., Sinova, J., Onoda, S., MacDonald, A.H. & Ong, N.P., *Anomalous Hall effect*, Rev. Mod. Phys., **82**, p. 1539, 2010.
[10] Sinova, J., Valenzuela, S.O., Wunderlich, J., Back, C.H. & Jungwirth, T., *Spin Hall effects*, Rev. Mod. Phys., **87**, p. 1213, 2015.
[11] Johansson, A., Herschbach, C., Fedorov, D.V., Gradhand, M. & Mertig, I., *Validity of the relativistic phase shift model for the extrinsic spin hall effect in dilute metal alloys*, J. Phys.: Condens. Matter, **26**, p. 274207, 2014.
[12] Xu, Z. Gu, B., Mori, M., Ziman, T. & Maekawa, S., *What determines the sign of the spin Hall effects in Cu alloys doped with 5d elements?* J. Magn. Magn. Mater., **400**, pp. 184-187, 2016.
[13] Liu, J., Ohkubo, T., Mitani, S., Hono, K. & Hayashi, M., *Correlation between the spin Hall angle and the structural phases of early 5d transition metals*, Appl. Phys. Lett., **107**, p. 232408, 2015.
[14] Kimura, T., Otani, Y., Sato, T., Takahashi, S. & Maekawa, S., *Room-temperature reversible spin Hall effect*, Phys. Rev. Lett., **98**, p. 156601, 2007.

[15] Guo, G.Y., Murakami, S., Chen, T.W. & Nagaosa, N., *Intrinsic spin Hall effect in platinum: First-principles calculations*, Phys. Rev. Lett., **100**, p. 096401, 2008.
[16] Keller, S., Mihalceanu, L., Schweizer, M.R., Lang, P., Heinz, B., Geilen, M., Bracher, T., Pirro, P., Meyer, T., Conca, A., Karfaridis, D., Vourlias, G., Kehagias, T., Hillebrands, B., & Papaioannou, E.T., *Determination of the spin Hall angle in single-crystalline Pt films from spin pumping experiments*, New J. Phys., **20**, p. 053002, 2018.
[17] Zhu, L., Zhu, L., Sui, M., Ralph, D.C., & Buhrman, R.A., *Variation of the giant intrinsic spin Hall conductivity of Pt with carrier lifetime*, Sci. Adv., **5** p. eaav8025, 2019.
[18] He, Y., Ji, Y. & Zhang, W., *Spin Hall conductivity in Pt films under tetragonal and orthorhombic distortions*, Physica B Condens. Matter, **605**, p. 412654, 2021.
[19] Fert, A. & Levy, P.M., *Spin Hall effect induced by resonant scattering on impurities in metals*. Phys. Rev. Lett., **106**, p. 157208, 2011.
[20] Tanaka, T., Kontani, H., Naito, M., Naito, T., Hirashima, D.S., Yamada, K. & Inoue, J., *Intrinsic spin Hall effect and orbital Hall effect in 4d and 5d transition metals*, Phys. Rev. B, **77**, p. 165117, 2008.
[21] Morota, M., Niimi, Y., Ohnishi, K., Wei, D.H., Tanaka, T., Kontani, H., Kimura, T. & Otani, Y., *Indication of intrinsic spin Hall effect in 4d and 5d transition metals*, Phys. Rev. B, **83**, p. 174405, 2011.
[22] Lowitzer, S., Gradhand, M., Ködderitzsch, D., Fedorov, D.V., Mertig, I. & Ebert, H., *Extrinsic and intrinsic contributions to the spin Hall effect of alloys*, Phys. Rev. Lett., **106**, p. 056601, 2011.
[23] Johnson, D.D., Pinski, F.J. & Staunton, J.B., *The Slater-Pauling curve: First principles calculations of the moments of* $Fe_{1-c}Ni_c$ *and* $V_{1-c}Fe_c$, J. Appl. Phys., **61**, p. 3715, 1987.
[24] Kakehashi, Y. & Hosohata, O., *Curie-temperature "Slater-Pauling curve"*, J. Phys. Colloq., **49** (C8), pp. C8–73, 1988.
[25] Takahashi, C., Ogura, M. & Akai, H., *First-principles calculation of the Curie temperature Slater-Pauling curve*, J. Phys.: Condens. Matter, **19**, p. 365233, 2007.
[26] Lowitzer, S., Kodderitzsch, D., Ebert, H. & Staunton, J.B., *Electronic transport in ferromagnetic alloys and the Slater-Pauling curve*, Phys. Rev. B, **79**, p. 115109, 2009.
[27] Nakamura, K., Ito, T., Freeman, A.J., Zhong, L. & Fernandez-de Castro, J., *Intra-atomic noncollinear magnetism and the magnetic structures of antiferromagnetic FeMn*, Phys. Rev. B, **67**, p. 014405, 2003.
[28] Perdew, J.P., Burke, K. & Ernzerhof, M., *Generalized Gradient Approximation made simple*, Phys. Rev. Lett., **77**, p. 3865, 1996.